

Surrogate-based cross-correlation for particle image velocimetry

Yong Lee,¹ Fuqiang Gu,² Zeyu Gong,³ Ding Pan,⁴ and Wenhui Zeng^{*4}

¹*School of Mechanical and Electronic Engineering, Wuhan University of Technology (WHUT), Wuhan 430070, China*

²*College of Computer Science, Chongqing University, Chongqing 400044, China*

³*State Key Laboratory of Intelligent Manufacturing Equipment and Technology, School of Mechanical Science and Engineering, Huazhong University of Science and Technology (HUST), Wuhan 430074, China*

⁴*School of Mechanical and Electronic Engineering, Wuhan University of Technology (WHUT), Wuhan 430070, China*

(*Electronic mail: zengwenhui3242@gmail.com)

(Dated: 21 May 2024)

This paper presents a novel surrogate-based cross-correlation (SBCC) framework to improve the correlation performance for practical particle image velocimetry (PIV). The basic idea is that an optimized surrogate filter/image, replacing one raw image, will produce a more accurate and robust correlation signal. Specifically, the surrogate image is encouraged to generate perfect Gaussian-shaped correlation map to tracking particles (PIV image pair) while producing zero responses to image noise (context images). And the problem is formularized with an objective function composed of surrogate loss and consistency loss. As a result, the closed-form solution provides an efficient multivariate operator that could consider other negative context images. Compared with the state-of-the-art baseline methods (background subtraction, robust phase correlation, etc.), our SBCC method exhibits significant performance improvement (accuracy and robustness) on the synthetic dataset and several challenging experimental PIV cases. Besides, our implementation with experimental details (<https://github.com/yonglee/SBCC>) is also available for interested researchers.

I. INTRODUCTION

Particle Image Velocimetry (PIV) is a popular non-intrusive instrument for flow field measurement in experimental fluid dynamics^{1–3}. PIV generates quantitative vector field by analyzing the consecutive particle recordings. However, the particle images are easily deteriorated in a practical measurement due to non-uniform light illumination, light reflections, background noise sources, camera dark noise, etc^{4–6}. Therefore, the accuracy and robustness of PIV results could be significantly decreased, recognized as *uncertainty*⁷, *peak-locking*⁸ and/or *outliers*^{9,10}. Thus, in this work, we focus on the challenging PIV estimation problem caused by the deteriorated particle recordings.

Over the past 40 years, the mainstream velocity estimation methods — cross-correlation^{11–15}, optical flow (OF)^{16–18} and deep neural-network (DNN) regression^{19–22} — are not particularly designed for robust PIV estimation. 1). The vanilla standard cross-correlation (SCC) computes the image similarity (dot product) as a function of the relative displacement. And SCC is not robust to image noise (such as, additive background noise, non-uniform illumination) because the noise is also correlated²³. Therefore, the generalized cross-correlation (GCC) methods improve signal-to-noise ratio of PIV cross-correlation via post-processing the correlation coefficients with different spectral filters, including phase correlation (PC)²⁴, symmetric phase-only filter (SPOF)²⁵, robust phase correlation (RPC)²³ to name a few. As a result, the GCC methods have achieved acceptable performance and have been extensively equipped for the majority of PIV software. 2). The optical flow¹⁶ methods employ a preservation principle, namely that particle image brightness attribute does not change after a movement, to estimate the particle displacement. The risk of failure rises if the brightness preser-

vation principle breaks, which often occurs with image noise in practical measurements. Thus, replacing the brightness attribute with other robust attributes (image gradient, image phase) could be a straightforward modification¹⁷. Besides, a deliberated OF model with improved regularization term also contributes to accurate PIV estimation^{18,26}. Meanwhile, the complex OF models often come with heavy computation cost. 3). As efficient inference methods, DNN-based regression methods^{19–21,27–29} have been attracting researchers' interest due to the powerful model capacity. However, the generalization of DNN for PIV depends on the noise type of training dataset³⁰. Totally speaking, the CC, OF, DNN can be treated as bivariate operators that only take in two particle image frames, regardless of the concrete noise signal of a measurement. Herein, we focus on the CC methods employed by most practitioners^{31–33}.

A straightforward alternative to achieve robust PIV analysis is to directly improve the image quality^{34–38}. Among different image pre-processing, the *background subtraction* performs well given a good reference background—concrete noise signal^{31,39–41}. The background image can either be recorded in the absence of seeding, or, if this is not possible, through temporal or spatial analysis from raw PIV recordings². The background image could be the minimum intensity image from double-frame PIV images, and works reliably for non-stationary flow with severe background noise^{4,5}. The varying background image could be extracted via a temporal Butterworth filter from a large number of raw PIV recordings⁶. A customized background can be adaptive reconstructed through proper orthogonal decomposition (POD)⁴⁰. Without extra temporal information, the spatial low-pass filter (LPF) utilizes the blur image to approximate a background, including Gaussian filter, median filter⁴², anisotropic diffusion⁴³, etc. Due to effectiveness, background subtraction has become an essential step of standard PIV pipeline (Fig. 1(a)). However, using one

background to model the complex noise signal is still challenging.

Correlation filters have achieved competitive success in object tracking by learning a discriminative linear tracker from several image templates^{44–46}. It generates an optimal filter/tracker that maximizes the convolution/tracking performance from multiple templates, as detailed in Section II. As a result of closed-form solution, correlation filter algorithm (minimum output sum of squared error, MOSSE⁴⁴) is not only easy to implement but significant faster. The extensive experiments exhibit that the learned filter outperforms the original image templates in both robustness and accuracy.

Our insight is that taking more negative context images (the concrete noise signal) into account will obtain a more robust tracker, and the MOSSE algorithm can be easily adapted to negative contexts with little effort. Different from object tracking video, the images of PIV pair are templates for each other⁴⁷. As a result, a novel surrogate-based cross correlation (SBCC) framework is proposed by combining forward surrogate tracking with backward surrogate tracking. And SBCC—a multivariate operator—enables us to reform PIV pipeline for accurate and robust measurement, rather than pursuing a perfect clean image (Fig. 1(b)). The main contributions are:

1. Inspired by the MOSSE filter, the SBCC is a new robust PIV analysis tool that employs several negative contexts, via robust surrogates and bi-directional consistency.
2. Based on MOSSE objective and bi-directional consistency formula, a concise closed-form solution to the problem is obtained. To our surprise, a set of widely-used *generalized cross-correlation* methods are special cases of the closed-form solution of SBCC framework.
3. The improvement of SBCC has been extensively verified on both synthetic and real PIV images.

The rest of this paper is arranged as follows. The related works are given in Section II. Section III describes our SBCC method from the problem formulation to optimization. And Section IV demonstrates the performance on synthetic datasets and real PIV images in comparison with baseline methods. Finally, the Section V remarks the paper with several concluding comments.

II. RELATED WORKS

A. Cross-correlations

The cross-correlation response $r(\mathbf{x})$ of image pair $f_1(\mathbf{x})$, $f_2(\mathbf{x})$ indicates the image displacement. Due to the Convolution Theorem, the computation of cross-correlation $r(\mathbf{x})$ becomes a fast element-wise multiplication in the Fourier frequency domain. That says, $R(\omega) = F_1(\omega)F_2^*(\omega)$, where $R(\omega)$, $F_1(\omega)$, $F_2(\omega)$ are the Fourier transform of $r(\mathbf{x})$, $f_1(\mathbf{x})$, $f_2(\mathbf{x})$ and the superscript (*) denotes complex conjugation. Hereafter, we will simplify the notations ($F_1(\omega)$, $F_2(\omega)$, ...) as

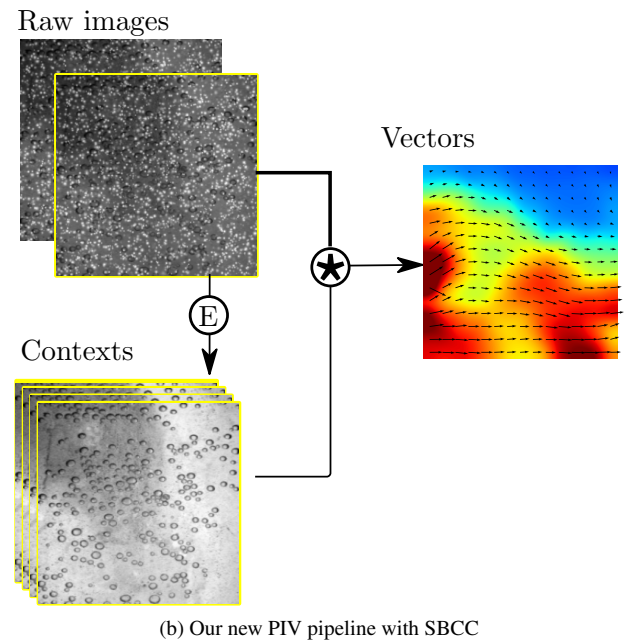
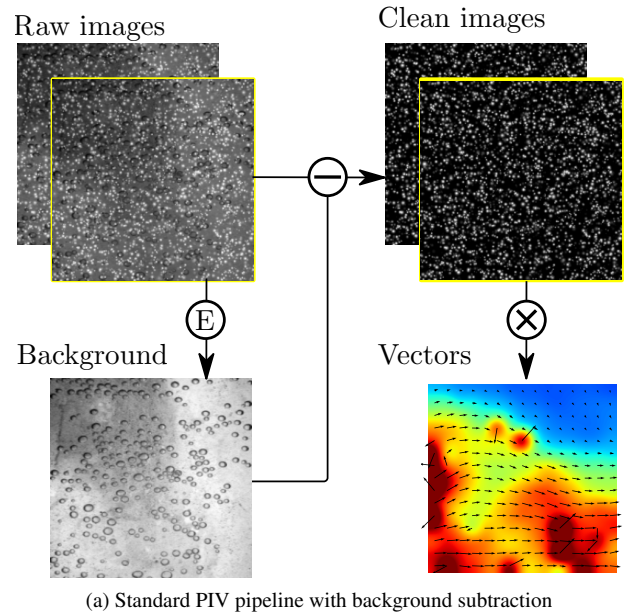


FIG. 1: Different illustrative pipelines for noisy PIV images.

ⓔ: background/contexts extraction; ⊖: background subtraction; ⊗: cross-correlation. ⊛: surrogate-based cross-correlation.

(F_1, F_2, \dots) by omitting the frequency ω . Due to its wide adoption in PIV estimation, this vanilla cross-correlation method will be referred to as the *standard cross-correlation* (SCC) method, as shown in Fig. 2 (a).

$$R_{SCC} = F_1 F_2^* \quad (1)$$

To enhance the correlation signal, the *generalized cross-correlation* (GCC) methods amend the SCC correlation R_{SCC}

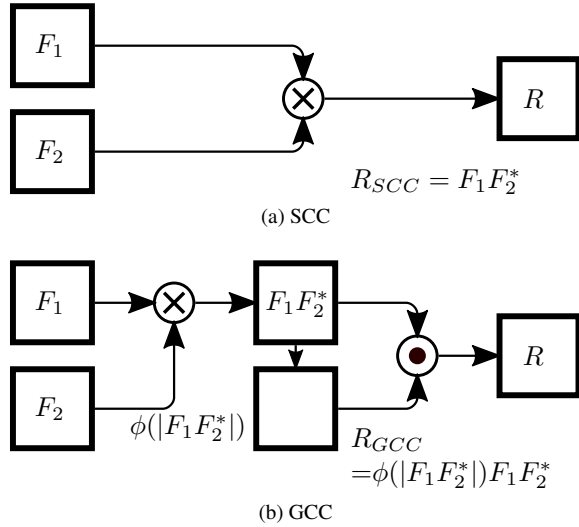


FIG. 2: Different cross-correlation methods. The \otimes denotes the standard cross-correlation in Fourier frequency domain (a). The generalized cross-correlation methods (b), the \odot represents an element-wise multiplication.

TABLE I: Different cross-correlation methods.

Methods	Equations	Comments
SCC ²	$R_{SCC} = F_1 F_2^*$	-
Pre-processing	$R_{PRE} = (H F_1)(H F_2)^*$	Filter H
Background subs	$R_{BGS} = (F_1 - B)(F_2 - B)^*$	Background B
PC ²⁴	$R_{PC} = \frac{F_1 F_2^*}{ F_1 F_2^* }$	GCC method
SPOF ²⁵	$R_{SPOF} = \frac{F_1 F_2^*}{\sqrt{ F_1 F_2^* }}$	GCC method
RPC ^{23,48}	$R_{RPC} = \frac{G F_1 F_2^*}{ F_1 F_2^* }$	GCC method
ρ -CSPC ⁴⁹	$R_{CSPC} = \frac{F_1 F_2^*}{ F_1 F_2^* ^\rho + \epsilon}$	GCC method
SBCC (ours)	$R_{SBCC} = \frac{2G F_1 F_2^*}{F_1 F_1^* + F_2 F_2^* + 2\mu \Sigma P_i P_i^*}$	Contexts P_i

with different spectral filters, i.e.,

$$R_{GCC} = \psi(F_1, F_2) F_1 F_2^* \quad (2)$$

where $\psi(\cdot)$ denotes the modification operation (PHAT filter²⁴, SPOF filter²⁵, RPC filter²³, etc.). Compared with the R_{PRE} (image pre-processing), the R_{GCC} can be viewed as a post-processing of $F_1 F_2^*$. Several GCC instances are listed in Table. I. The filters of these GCC methods share a special type, $\psi(F_1, F_2) = \phi(|F_1 F_2^*|)$, as demonstrated in Fig. 2 (b).

B. Correlation filter

The correlation filter can be derived either from an objective function specifically formularized in the Fourier domain⁴⁴ or from ridge regression and circulant matrices⁴⁵. Slightly different from^{44,45}, we provide our understanding of correlation filter as following. Given a set of aligned template images

$T_i, i \in \{1, 2, \dots, n\}$, the MOSSE method^{44,45} finds a surrogate filter/tracker S that produces the best tracking performance, i.e., the cross-correlation response $r_i(\mathbf{x}) = \mathcal{F}^{-1}(T_i S^*)$ is encouraged to be an isotropic Gaussian-shaped response $g(\mathbf{x})$, where $\mathcal{F}^{-1}(\cdot)$ denotes inverse fourier transform. In addition, a regularization term $|S|^2$ is employed to avoid the over fitting and gains the stability, similar to Wiener filtering or ridge regression⁴⁵. Hence, the minimum output sum of squared error (MOSSE) objective arrives,

$$J_{MOSSE}(S) = \sum_{i=1}^n |G - T_i S^*|^2 + \mu |S|^2 \quad (3)$$

where μ controls the amount of regularization, and it is recommended to be 0.1⁴⁴. The n is the number of positive templates, and G denotes the Fourier transform of a Gaussian function $g(\mathbf{x})$. A closed-form solution of MOSSE,

$$\hat{S}^* = \frac{\sum_i G T_i^*}{\sum_i T_i T_i^* + \mu} \quad (4)$$

The μ plays an important role to make the denominator not equal to zero. Interestingly, the numerator is the correlation between the input and the desired output and the denominator is the energy spectrum of the input.

Our observation is that the regularization term of Eq.(3), $|S|^2 = |0 - 1 \cdot S^*|^2$, could be regarded as a special term for a negative template (delta function, $1 \Leftrightarrow \delta(\mathbf{x})$). That is to say, the MOSSE filter also expects the cross-correlation between S and a negative Dirac delta function to be zero. Now, it is clear that the parameter μ controls the relative importance for this negative template response.

III. SURROGATE-BASED CROSS-CORRELATION

A. Problem formulation

As mentioned in Section I, the standard PIV pipeline might fail due to one limited background image. We thus introduce the surrogate-based cross-correlation which utilizes multiple context background images to enhance particles correlation. Specifically, a surrogate filter/image (S_1 or S_2) is assumed to have a better cross-correlation response under a well-designed surrogate objective J_{surr} , which considers the tracking performance as well as robustness. Meanwhile, similar to ensemble correlation, the forward correlation response R_f (with surrogate S_1) and backward response R_b (with surrogate S_2) are combined via correlation consistency objective J_{corr} . Thus, the robust PIV estimation problem is formulated with two objectives, as illustrated in Fig. 3,

$$\hat{R}, \hat{S}_1, \hat{S}_2 = \arg \min_{R, S_1, S_2} J_{SBCC}(R, S_1, S_2; F_1, F_2) \quad (5)$$

with

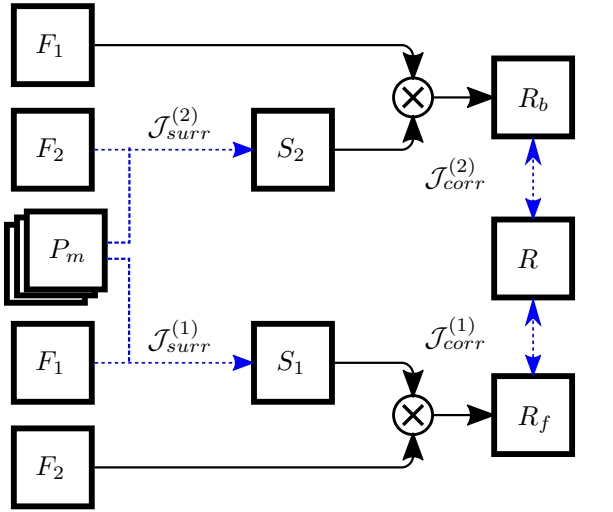


FIG. 3: The bi-directional surrogate model, SBCC. The surrogate images S_1, S_2 and correlation response R are jointly optimized with surrogate objective J_{surr} and correlation consistency objective J_{corr} (blue dash arrows). The R_f and R_b represent the correlation with forward surrogate (S_1) and backward surrogate (S_2) respectively.

$$\begin{aligned}
 J_{SBCC}(R, S_1, S_2; F_1, F_2) &= \underbrace{J_{surr}(S_1; F_1) + J_{surr}(S_2; F_2)}_{\text{surrogate objective}} \\
 &+ \underbrace{J_{corr}(R_f, R) + J_{corr}(R_b, R)}_{\text{correlation consistency objective}}
 \end{aligned} \quad (6)$$

where $R_f = S_1 F_2^*$, $R_b = F_1 S_2^*$ are the forward correlation response and backward correlation response. Note that the surrogates S_1, S_2 are no longer the processed results of image pre-processing due to the coupled SBCC structure.

Surrogate objective. To gain robustness of surrogate filter, a well-designed surrogate objective is thus constructed, which makes use of the positive template and other negative context images. The negative samples are proved to be useful for representation learning⁵⁰. Similar to MOSSE⁴⁴, our surrogate objective J_{surr} (Fig. 4) is given before a detail explanation,

$$\begin{aligned}
 J_{surr}(S; F) &= \underbrace{|G - FS^*|^2}_{\text{MOSSE term}} + \underbrace{\mu \frac{1}{m} \sum_{i=1}^m |0 - P_i S^*|^2}_{\text{negative context term}} \\
 &= |G - FS^*|^2 + \mu \frac{1}{m} \sum_{i=1}^m |P_i S^*|^2
 \end{aligned} \quad (7)$$

where $P_i, i \in \{1, 2, \dots, m\}$ are the negative context images. The G denotes the Fourier transform of Gaussian functions $g(\mathbf{x})$. The μ is also the coefficient for the negative context term. The MOSSE term is preserved to encourage a Gaussian-shaped correlation map. Reducing the filter's response to the background/noise could decrease the number of outliers, because

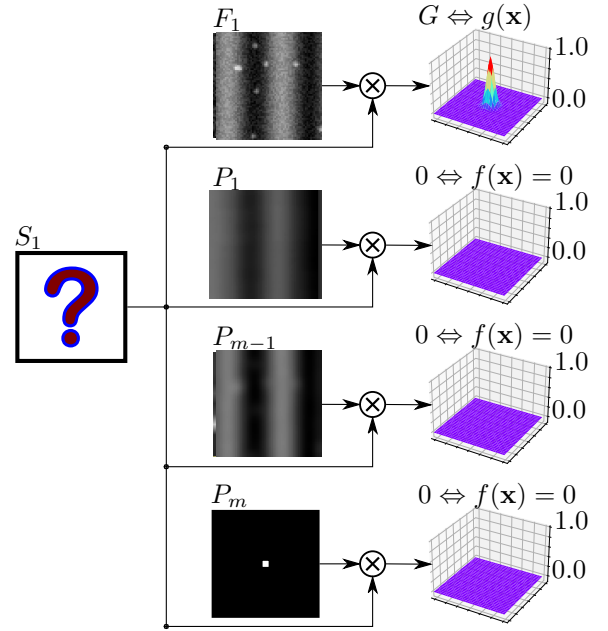


FIG. 4: The motivation of surrogate objective is to find a surrogate S_1 that does not response to the negative context images P_1, P_2, \dots, P_m .

most outliers occur when the images have similar image background or other noisy pattern. Recall that the regularization term $|S|^2$ of MOSSE, it encourages the surrogate filter S produce zero response to the special $\delta(\mathbf{x})$. However, the negative context term of Eq. (7) encourages the filter S produce zero response to all context images. We choose the backgrounds from temporal minimum value (MIN bg) and spatial low-pass results (LPF bg) as the context images in this work. Obviously, other options are also supported. Compared to the $\delta(\mathbf{x})$, the context images are more likely to have a similar noisy pattern with PIV test images.

Correlation consistency objective. Different from object tracking, the paired images of PIV can be treated as templates to each other. Our SBCC framework (Fig. 3) models it as forward and backward correlation. To obtain a consistency result, a square error encourages a minimum distance between $R_x \in \{R_b, R_f\}$ to the final correlation map R .

$$J_{corr}(R_x, R) = |R - R_x|^2 \quad (8)$$

Recall $R_f = S_1 F_2^*$, $R_b = F_1 S_2^*$ are the forward correlation response and backward correlation response, and R is the final cross-correlation response of SBCC.

Take the *surrogate objective* (Eq. (7)) and *correlation consistency objective* (Eq. (8)) back into the problem (Eq. (6)).

The specific objective function of SBCC is arrived,

$$\begin{aligned}
J_{SBCC}(R, S_1, S_2; F_1, F_2) &= |G - F_1 S_1^*|^2 + \mu \frac{1}{m} \sum_{i=1}^m |P_i S_1^*|^2 \\
&+ |G - F_2 S_2^*|^2 + \mu \frac{1}{m} \sum_{i=1}^m |P_i S_2^*|^2 \\
&+ |R - S_1 F_2^*|^2 + |R - F_1 S_2^*|^2
\end{aligned} \quad (9)$$

This objective is the sum of several squared errors with three unknown complex variables S_1, S_2, R . The parameter μ controls the relative importance of the negative context images.

B. Optimization of SBCC objective

The optimization of J_{SBCC} (Eq. 9) is almost identical to the optimization problems in^{44,45}. The difference is that SBCC objective is a quadratic convex function with three complex variables. The closed-form solution thus can be found by setting the partials to zeroes,

$$\begin{aligned}
R_{SBCC} := \hat{R} &= \frac{2GF_1 F_2^*}{F_1 F_1^* + F_2 F_2^* + 2\mu Q} \\
\hat{S}_1 &= \frac{F_2 \hat{R} + GF_1}{F_1 F_1^* + F_2 F_2^* + \mu Q} \\
\hat{S}_2^* &= \frac{F_1^* \hat{R} + GF_2^*}{F_1 F_1^* + F_2 F_2^* + \mu Q}
\end{aligned} \quad (10)$$

where $Q = \frac{1}{m} \sum_{i=1}^m P_i P_i^*$ is the average Fourier power spectrum of negative context images. The cross-correlation response, R_{SBCC} , incorporates this Q component to obtain a robustness correlation by considering the noisy background in these negative context images. The terms in R_{SBCC} (Eq. (10)) have clear interpretation. The numerator is the cross-correlation between F_1 and F_2 with a Gaussian filter (G), and the denominator is the power spectrum sum of F_1 , F_2 , and negative context images P_i . Note that the \hat{S}_1 depends on F_1 as well as F_2 .

C. Short discussion

Due to the clear meaning of the objective function J_{SBCC} , the solution R_{SBCC} has good interpretation as well. Observing the SBCC solution, we found that a set of hand-crafted GCC methods are special cases of SBCC. That is to say, our SBCC framework provides a new perspective to understand existing GCC methods (Table. I).

Firstly, we consider a simple but useful equation,

$$F_1 F_1^* + F_2 F_2^* = (|F_1| - |F_2|)^2 + 2|F_1 F_2^*| \geq 2|F_1 F_2^*| \quad (11)$$

Thus, the mathematical representation of PC, RPC, 1-CSPC become special SBCC cases with an impractical noise-free as-

sumption ($|F_1| = |F_2|$). That says,

$$\begin{aligned}
R_{PC} &= R_{SBCC}|_{G=1, |F_1|=|F_2|, \mu=0} \\
R_{1-CSPC} &= R_{SBCC}|_{G=1, |F_1|=|F_2|, \mu=\epsilon, P_i=1} \\
R_{RPC} &= R_{SBCC}|_{G \leftrightarrow g(x), |F_1|=|F_2|, \mu=0}
\end{aligned} \quad (12)$$

which means that, PC and 1-CSPC encourage a Dirac delta response ($G = 1$), while RPC method expects a Gaussian-shaped response. Only 1-CSPC method has considered a special context image $\delta(\mathbf{x})$ implicitly. However, all methods employ a noise-free assumption ($|F_1| = |F_2|$).

The SPOF is beyond a brief understanding. However, the SPOF can be treated as an ensemble correlation⁵¹ due to the following relationship, $R_{SPOF} R_{SPOF} = R_{SCC} R_{PC}$. It might imply that multiple SBCC frameworks can provide more complex surrogate for SPOF and general ρ -CSPC methods. Note that none of the existing GCC methods explicitly take any negative context images into consideration.

IV. EXPERIMENTS

In this section, the performance of SBCC is extensively evaluated through visualizing the correlation map, analysing parameter sensitivity, conducting measurement on synthetic images and experimental PIV images. The detailed implementation and additional results are provided at the project repository, <https://github.com/yongleex/SBCC>.

Baseline methods. Several widely-accepted approaches are adopted to conduct a fair evaluation. And they are, standard cross-correlation (SCC)², symmetric phase-only filter (SPOF)²⁵, robust phase correlation (RPC)²³. Regarding the background subtraction methods, we choose the minimum intensity image from double-frame PIV image⁴ and the spatial low-pass filter (LPF)⁴², resulting in SCC-MIN and SCC-LPF. To exclude the influence of other factors, single-pass cross-correlation without any post-processing is utilized for all testing methods.

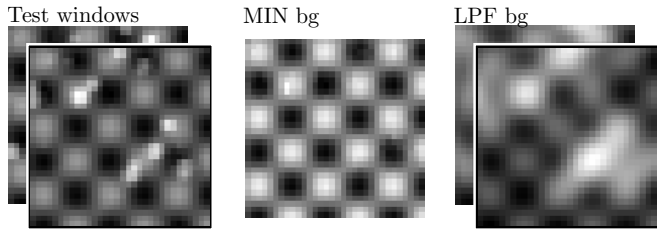
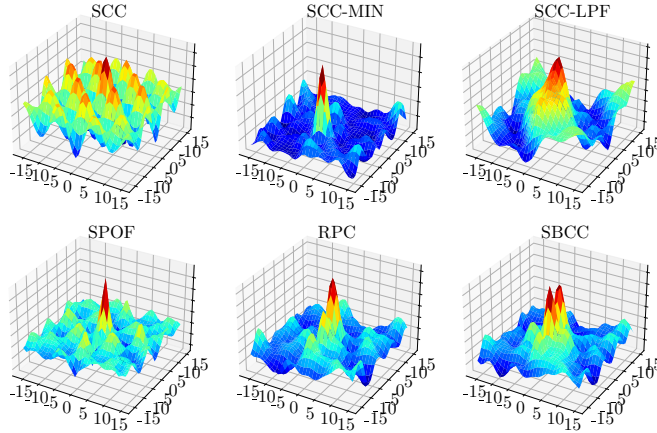
Evaluation criteria. In addition to subjective visual judgement, three objective metrics are also employed to quantify the performance: 1) the root mean-square-error (RMSE)^{2,3,19}, 2) the average endpoint error (AEE)²¹, 3) the execution time for different image size.

$$\begin{aligned}
RMSE &= \sqrt{\frac{1}{N} \sum_{i=1}^N \|\mathbf{v}_{e,i} - \mathbf{v}_{t,i}\|^2} \\
AEE &= \frac{1}{N} \sum_{i=1}^N \|\mathbf{v}_{e,i} - \mathbf{v}_{t,i}\|
\end{aligned} \quad (13)$$

where $\mathbf{v}_{e,i} = (v_x, v_y)$ is the i^{th} estimated vector out of N points, while the $\mathbf{v}_{t,i}$ denotes the i^{th} ground truth.

A. On correlation coefficients

Fig. 5 (a) gives a test pair of synthetic PIV interrogation window (particle displacement is $-5.0pixel$ in horizontal),

(a) A test image pair ($u = -5.0\text{pixel}$) and estimated backgrounds

(b) The correlation maps

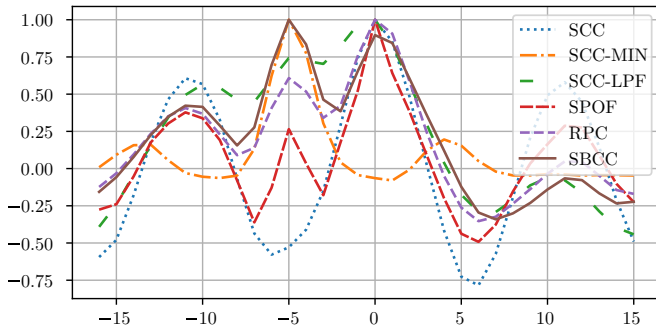
(c) The correlation coefficient at $\Delta y = 0$

FIG. 5: A correlation responses on synthetic particle images with background. Best viewed in color.

with a unrealistic strong additive background. Obviously, the minimum intensity image (MIN bg) recovers the still background, while the LPF (LPF bg) can not tell the background and particle image apart due to frequency aliasing.

Fig. 5 (b) and (c) provide the cross-correlation coefficients for this challenging synthetic case. The SCC, SPOF, RPC fail to obtain the correct response peak due to a lack of noise signal. Although the SCC-LPF method does not show the correct peak, the rough background also helps to increase the image similarity at the correct displacement. Without surprising, the SCC-MIN method is demonstrated with perfect correlation peak with good background estimation in this case. Compared to other methods, the SBCC has a correlation map with two distinct peaks, and correlation peak (maximum similarity) is correctly located at $(-5.0, 0.0)$. Closing observing the curve around $(-5.0, 0.0)$, the SBCC has a similar landscape with

SCC-MIN. Thus, we can conclude that SBCC provides another feasible mechanism to perform robust cross-correlation with the help of background signals.

B. On parameter sensitivity

The only parameter μ needs to be determined for our SBCC method working at the best condition. Similar to the background subtraction, it's very difficult to obtain ideal context images. Hence, increasing μ will not always benefit the robustness or accuracy. We thus argue that there is an optimal parameter μ for the practical PIV measurement.

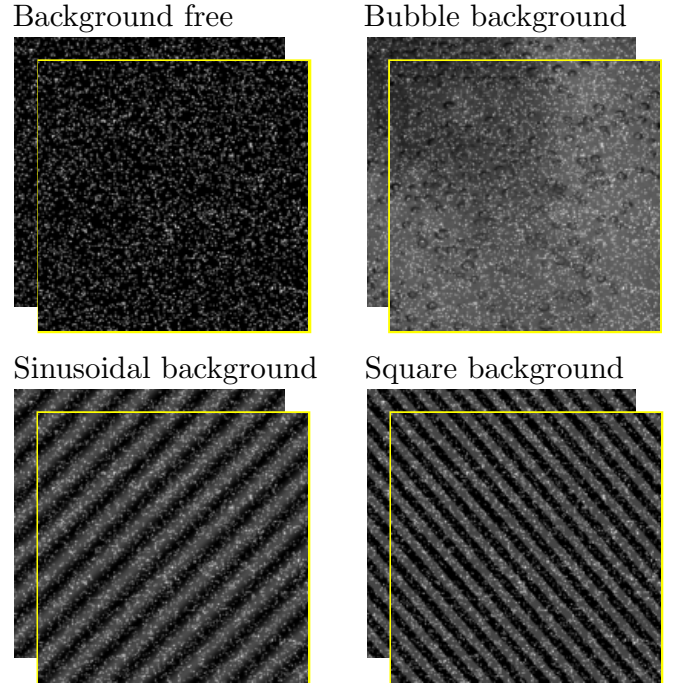
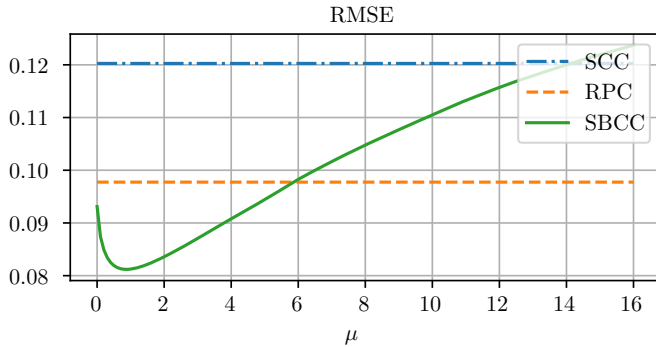


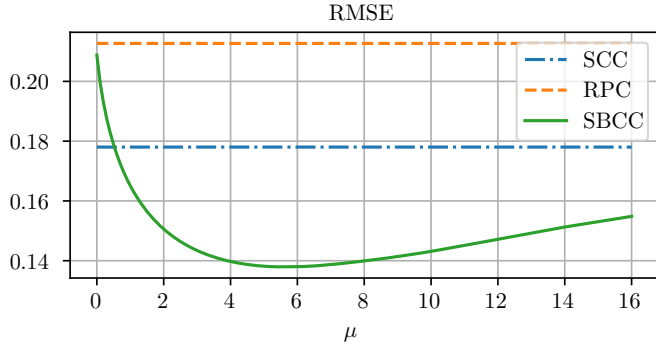
FIG. 6: Synthetic particle images with/without different backgrounds (uniform flow).

To study the effect of different μ values, we also employ the synthetic particle images from particle image generator (PIG). Here, we use a subset of a ready dataset (1000 uniform flow)^{20,52}. Different from the noise-free images, a random synthetic image is added to the clean synthetic image pair, to simulate the still background. The background images are from a bubble dataset (1219 images of class 1)^{53,54}, synthetic sinusoidal and square signal, as demonstrated in Fig. 6.

Fig. 7 illustrates the experimental results with both background-free and bubble background image pair (top row of Fig. 6) respectively, and the parameter μ varies from 0 to 16 with interval 0.1. In comparison with noise-free case, the RMSE of all methods are increased when additive bubble noise is added. It reflects the PIV challenge caused by the unwanted background. Interestingly, the sensitivity curve of SBCC have an optimal value that corresponds with the minimum RMSE value. The optimal value μ of complex background is larger than that of background-free situation. Mean-



(a) RMSE for a background-free image pair



(b) RMSE for an image pair with bubble background

FIG. 7: Effect of the parameter μ of SBCC. ($u = 0.85 \text{ pixel}$, $v = 1.23 \text{ pixel}$)

while, an improvement of SBCC happens for a large range of μ , i.e., range $[0, 6]$ for background-free and $[1, 16]$ for bubble background. Thus, setting a proper μ could be an interesting problem for future work. Anyway, we set μ to 3.0 arbitrarily by taking all cases into consideration based on the results of this experiment. Note that, the fixed $\mu(3.0)$ is not changed for different measurement cases, and the extensive results illustrate that this value could have a universal robust performance.

C. On synthetic PIV images

TABLE II: Synthetic experiment on one image pair. Performance measured by RMSE. The best **in Bold**.

Background	Free	Bubble	Sinusoidal	Square
SCC	0.3753	0.5054	0.7930	0.4644
SCC-MIN	0.4422	0.4422	0.4422	0.4422
SCC-LPF	0.3919	0.3487	0.3934	0.3244
SPOF	0.4060	0.4530	0.4725	0.4382
RPC	0.1883	0.6597	0.3724	0.2274
SBCC	0.2195	0.2765	0.1914	0.1985

To quantitatively compare the performance, a synthetic image pair is sampled²⁰ with different backgrounds (Fig. 6). Table II and III give the RMSE and AEE values for the processed results. For the background-free scenario, vanilla SCC

TABLE III: Synthetic experiment on one image pair. Performance measured by AEE. The best **in Bold**.

Background	Free	Bubble	Sinusoidal	Square
SCC	0.3422	0.4557	0.7813	0.4311
SCC-MIN	0.3827	0.3827	0.3827	0.3827
SCC-LPF	0.3438	0.3213	0.3721	0.3054
SPOF	0.3768	0.4181	0.4460	0.4099
RPC	0.1619	0.4193	0.3440	0.1983
SBCC	0.2050	0.2457	0.1741	0.1810

yields satisfactory result, while the variations (SCC-MIN, SCC-LPF and SPOF) do not show a consistent improvement in accuracy. For the cases with background, all variants have a better performance than SCC. It implies that background subtraction (SCC-MIN, SCC-LPF) and spectral filters (SPOF, RPC) are all effective to address background problem. In this experiment, the RPC has the smallest measurement error on background-free images, while SBCC achieves significant improvement for the cases with background.

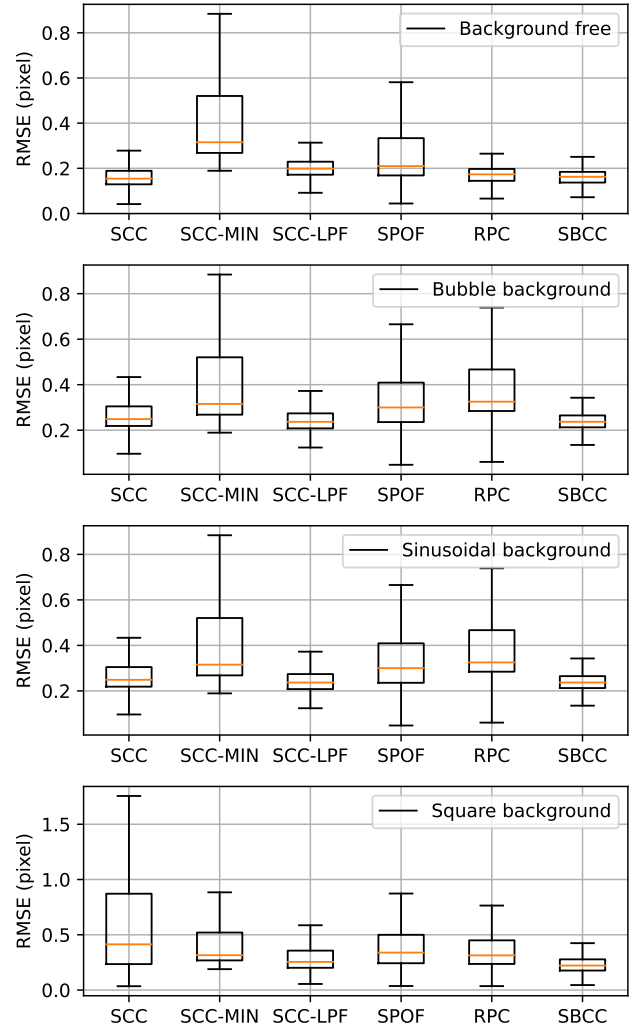


FIG. 8: Boxplot of the RMSE for the synthetic 1000 uniform cases with 4 types of backgrounds and 6 PIV CC estimators.

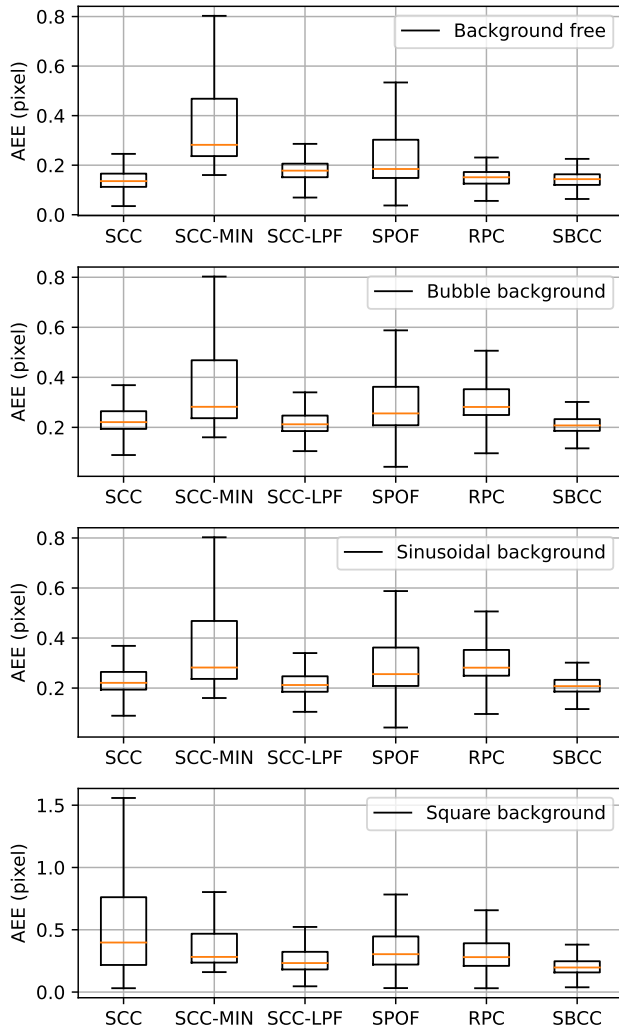
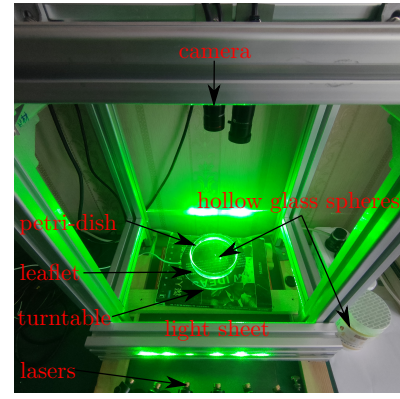
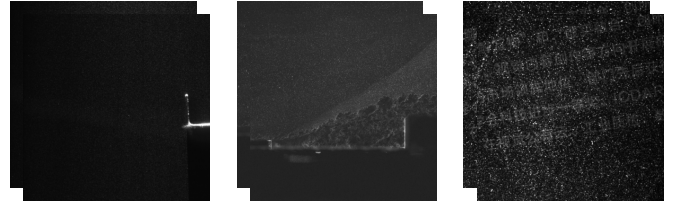


FIG. 9: Boxplot of the AEE for the synthetic 1000 uniform cases with 4 types of backgrounds and 6 PIV CC estimators.

In addition to case study, the Monte Carlo simulation is widely adopted in the assessment of PIV measurement uncertainty^{2,19}. Recall that, the 1000 synthetic particle image pairs (256×256 pixel²) are synthesized with uniform flows ground truth⁵², and the backgrounds are sampled from a bubble dataset⁵⁴ and two artificial signals (random sinusoidal wave and square wave). The boxplots in Fig. 8 and 9 present the statistical results of 1000 cases measured by RMSE and AEE. The one-pass SCC and RPC method have acceptable measurement error (RMSE ~ 0.2) for background-free cases due to varying seeding density, particle diameters, illuminations in the image generator. However, they are not robust enough to backgrounds. Both SCC-MIN and SPOF have poor performance on all cases. The reasons might be the low-quality background of SCC-MIN, while peak-locking causes a significant error of SPOF. On the contrary, both SCC-LPF and SBCC performs well for all test cases. We speculate that the synthetic backgrounds might be well estimated by a LPF, resulting in the good performance of SCC-LPF. Note that, our SBCC is more accurate than SCC-LPF statistically.



(a) A lab-made PIV setup with an industrial camera (HIKROBOT, MV-CA016-10UM) and multiple semiconductor lasers (532nm)



(b) Left: interactive flow around L-shaped plate³²; Middle: hypersonic flow over a step model⁵⁵; Right: rotational flow with background from (a).

FIG. 10: A lab-made setup (a) and 3 practical test cases (b).

D. On real recorded PIV images

In addition to synthetic images, we also tested SBCC on three challenging recorded PIV image pairs (Fig. 10 (b)). The first case records an interactive flow around L-shaped plate in OpenPIV³². The second PIV case records a hypersonic flow ($5Ma$) over a step model⁵⁵. The third image pair is from a lab-made PIV setup (Fig. 10 (a)), which represents a liquid column rotating with a still text leaflet background (similar to PIV Challenge 2014, Case F). These flows have particular structures with large displacement (≈ 10 pixel), and the images have non-uniform illumination, out-of-plane effects and noise background. Thus, they are considered as the challenging test examples.

Fig. 11, 12 and 13 provide the raw vector field results, computed with different one-pass cross-correlation methods without any post-processing operation. The pseudo-color backgrounds represent the vector magnitudes. Overall, different methods output similar flow patterns, verifying that these widely-used methods do work in practice. Unfortunately, the accuracy for each method can not be exactly assessed due to unknown ground truth. Thus, we visually check the outliers for the problematic areas in white boxes to evaluate the robustness of each method. The left area of interactive flow image is under weak illumination, and thus full of random noise. The results indicate the spectral filters (SPOF, RPC and SBCC) can effectively cope with this problem, as reported in related works²³. The middle box of hypersonic flow, with strong out-of-plane movement, is full of uncorrelated particles. We ar-

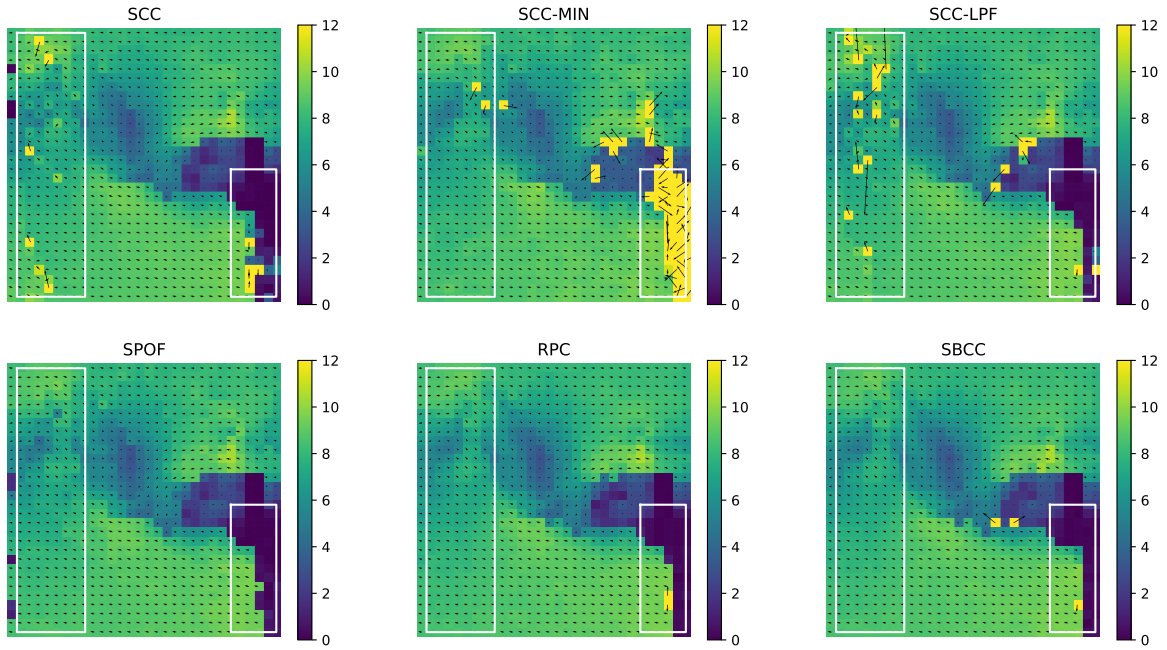


FIG. 11: Vectors from the interactive flow. The color background corresponds to velocity magnitude. Best viewed in color.

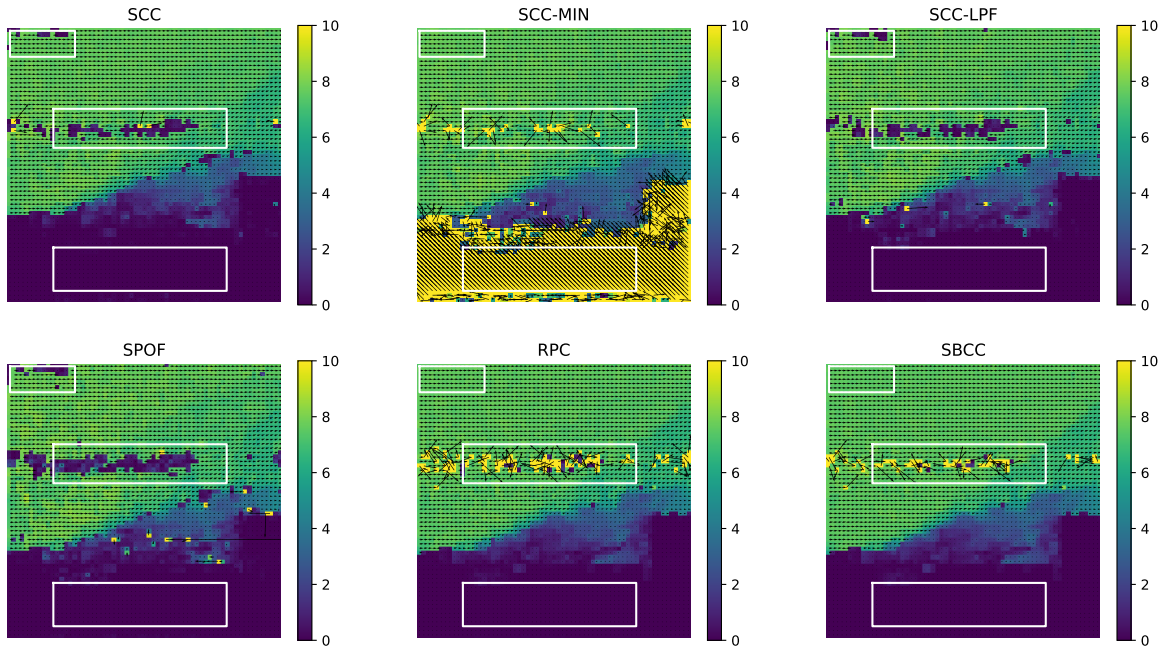


FIG. 12: Vectors from the hypersonic flow. The color background corresponds to velocity magnitude. Best viewed in color.

gue that the MIN background could catch some content of the noise signal, resulting in the less outliers of SCC-MIN and SBCC. The complex background of rotational flow is obviously difficult to reconstruct with MIN or LPF approaches, which explains the bad performance of SCC-MIN and SCC-LPF. Besides, the spectral filter of RPC also does not work well for this case. However, combining multiple background contexts and spectral filter, our SBCC has an impressive performance with a few outliers for this strong background of

advertising words. Based on the impressive results of comprehensive (synthetic and recorded) experiments, the overall effectiveness of our SBCC has been confirmed.

E. On computing cost

To demonstrate the efficiency of proposed SBCC, the baseline methods and SBCC were finally tested using Python 3.8

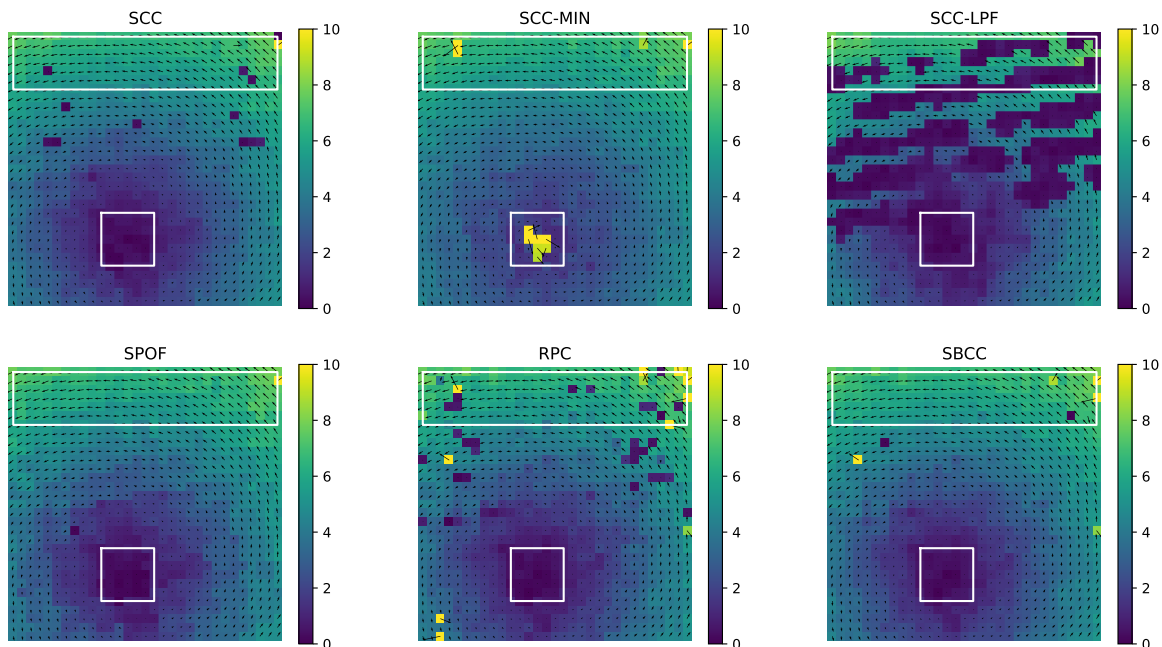


FIG. 13: Vectors from the rotational flow. The color background corresponds to velocity magnitude. Best viewed in color.

TABLE IV: The running time (seconds) (averaged over 10 runs, with standard deviations).

Image size	128×128	256×256	512×512	1014×1024
SCC	0.0022 ± 0.0002	0.0055 ± 0.0009	0.0233 ± 0.0019	0.0792 ± 0.0031
SCC-MIN	0.0020 ± 0.0005	0.0055 ± 0.0007	0.0220 ± 0.0009	0.0785 ± 0.0026
SCC-LPF	0.0070 ± 0.0127	0.0081 ± 0.0008	0.0277 ± 0.0006	0.0838 ± 0.0030
SPOF	0.0019 ± 0.0001	0.0071 ± 0.0004	0.0232 ± 0.0005	0.0834 ± 0.0032
RPC	0.0022 ± 0.0002	0.0067 ± 0.0002	0.0232 ± 0.0007	0.0822 ± 0.0024
SBCC	0.0070 ± 0.0034	0.0187 ± 0.0004	0.0576 ± 0.0034	0.1995 ± 0.0315

on a 2.70GHz i5-11400H laptop computer (HP OMEN 16) with RAM 16.00GB. Tested over 10 runs, the execution results (Table. IV) with varied image size demonstrated that the SBCC has an acceptable computational cost. Recall that an extra FFT operation of contexts is needed, and it is worthwhile to cost $2 \sim 3$ times computation for the accuracy improvement. For a 1024×1024 case, the execution time of our SBCC is less than 0.2 second.

V. CONCLUSION

Inspired by correlation filter, a novel SBCC framework is proposed to enhance the cross-correlation performance by incorporating multiple negative context images. As a multivariate operator, the SBCC is the closed-form solution of a well-designed optimization problem, which is formulated with both surrogate objective and correlation consistency objective. To our surprising, this framework also provides an alternative surrogate view for a set of generalized cross-correlation methods (PC, RPC, 1-CSPC, SPOF, etc). On the correlation response, the SBCC method is more likely to achieve a desired Gaussian-shaped correlation response, encouraged by the ob-

jective function. And an arbitrary parameter $\mu(3.0)$ is fixed through parameter sensitivity analysis. Finally, the performance improvement of SBCC is verified with massive synthetic and real PIV image pairs. An interesting point is that SBCC paves a new way for robust PIV cross correlation analysis via employing negative context images. Moving forward, we plan to apply SBCC beyond PIV to other tasks including one-dimensional time series, digital image correlation, acoustic imaging, etc.

ACKNOWLEDGMENT

This work was supported by the National Natural Science Foundation of China (Grant No.: 52205575), Natural Science Foundation of Hubei Province (Grant Number: 2023AFB128) and Teaching Research Project of Wuhan University of Technology (Grant Number: W2022093). The authors would like to thank Dr. B. Wieneke and Zhenghao Cen for beneficial discussion.

DATA AVAILABILITY STATEMENT

The data that support the findings of this study are available from the corresponding author upon reasonable request.

- ¹R. J. Adrian, “Scattering particle characteristics and their effect on pulsed laser measurements of fluid flow: speckle velocimetry vs particle image velocimetry,” *Applied optics* **23**, 1690–1691 (1984).
- ²M. Raffel, C. E. Willert, F. Scarano, C. J. Kähler, S. T. Wereley, and J. Kompenhans, *Particle image velocimetry: a practical guide* (Springer, 2018).
- ³Y. Lee and S. Mei, “Diffeomorphic particle image velocimetry,” *IEEE Transactions on Instrumentation and Measurement* **71** (2022).
- ⁴M. Honkanen and H. Nobach, “Background extraction from double-frame piv images,” *Experiments in fluids* **38**, 348–362 (2005).
- ⁵N. G. Deen, P. Willems, M. van Sint Annaland, J. Kuipers, R. G. Lammerntink, A. J. Kemperman, M. Wessling, and W. G. van der Meer, “On image pre-processing for piv of single- and two-phase flows over reflecting objects,” *Experiments in fluids* **49**, 525–530 (2010).
- ⁶A. Sciacchitano and F. Scarano, “Elimination of piv light reflections via a temporal high pass filter,” *Measurement Science and Technology* **25**, 084009 (2014).
- ⁷A. Sciacchitano, “Uncertainty quantification in particle image velocimetry,” *Measurement Science and Technology* **30**, 092001 (2019).
- ⁸D. Michaelis, D. R. Neal, and B. Wieneke, “Peak-locking reduction for particle image velocimetry,” *Measurement Science and Technology* **27**, 104005 (2016).
- ⁹H. Wang, Q. Gao, L. Feng, R. Wei, and J. Wang, “Proper orthogonal decomposition based outlier correction for piv data,” *Experiments in Fluids* **56**, 1–15 (2015).
- ¹⁰Y. Lee, H. Yang, and Z. Yin, “Outlier detection for particle image velocimetry data using a locally estimated noise variance,” *Measurement Science and Technology* **28**, 035301 (2017).
- ¹¹C. E. Willert and M. Gharib, “Digital particle image velocimetry,” *Experiments in fluids* **10**, 181–193 (1991).
- ¹²F. Scarano, “Iterative image deformation methods in piv,” *Measurement science and technology* **13**, R1 (2001).
- ¹³H. Wang, G. He, and S. Wang, “Globally optimized cross-correlation for particle image velocimetry,” *Experiments in Fluids* **61**, 1–17 (2020).
- ¹⁴X. Zhu, C. Xu, M. M. Hossain, J. Li, B. Zhang, and B. C. Khoo, “Approach to select optimal cross-correlation parameters for light field particle image velocimetry,” *Physics of Fluids* **34** (2022).
- ¹⁵Q. Gao, H. Lin, H. Tu, H. Zhu, R. Wei, G. Zhang, and X. Shao, “A robust single-pixel particle image velocimetry based on fully convolutional networks with cross-correlation embedded,” *Physics of Fluids* **33** (2021).
- ¹⁶T. Corpetti, D. Heitz, G. Arroyo, E. Mémin, and A. Santa-Cruz, “Fluid experimental flow estimation based on an optical-flow scheme,” *Experiments in fluids* **40**, 80–97 (2006).
- ¹⁷Q. Zhong, H. Yang, and Z. Yin, “An optical flow algorithm based on gradient constancy assumption for piv image processing,” *Measurement Science and Technology* **28**, 055208 (2017).
- ¹⁸J. Lu, H. Yang, Q. Zhang, and Z. Yin, “An accurate optical flow estimation of piv using fluid velocity decomposition,” *Experiments in Fluids* **62**, 1–16 (2021).
- ¹⁹Y. Lee, H. Yang, and Z. Yin, “Piv-dcnn: cascaded deep convolutional neural networks for particle image velocimetry,” *Experiments in Fluids* **58**, 171 (2017).
- ²⁰S. Cai, S. Zhou, C. Xu, and Q. Gao, “Dense motion estimation of particle images via a convolutional neural network,” *Experiments in Fluids* **60**, 1–16 (2019).
- ²¹C. Lagemann, K. Lagemann, S. Mukherjee, and W. Schröder, “Deep recurrent optical flow learning for particle image velocimetry data,” *Nature Machine Intelligence* **3**, 641–651 (2021).
- ²²L. Cao, M. M. Hossain, J. Li, and C. Xu, “Three-dimensional particle image velocimetry measurement through three-dimensional u-net neural network,” *Physics of Fluids* **36** (2024).
- ²³A. Eckstein and P. P. Vlachos, “Digital particle image velocimetry (dpiv) robust phase correlation,” *Measurement Science and Technology* **20**, 055401 (2009).
- ²⁴J. L. Horner and P. D. Gianino, “Phase-only matched filtering,” *Applied optics* **23**, 812–816 (1984).
- ²⁵M. P. Wernet, “Symmetric phase only filtering: a new paradigm for dpiv data processing,” *Measurement Science and Technology* **16**, 601 (2005).
- ²⁶L. Bao, Q. Yang, and H. Jin, “Fast edge-preserving patchmatch for large displacement optical flow,” in *Proceedings of the IEEE Conference on Computer Vision and Pattern Recognition* (2014) pp. 3534–3541.
- ²⁷M. Zhang and M. D. Piggott, “Unsupervised learning of particle image velocimetry,” in *High Performance Computing: ISC High Performance 2020 International Workshops, Frankfurt, Germany* (Springer, 2020) pp. 102–115.
- ²⁸C. Yu, X. Bi, Y. Fan, Y. Han, and Y. Kuai, “Lightpivnet: An effective convolutional neural network for particle image velocimetry,” *IEEE Transactions on Instrumentation and Measurement* (2021).
- ²⁹C. Yu, Y. Fan, X. Bi, Y. Kuai, and Y. Chang, “Deep dual recurrence optical flow learning for time-resolved particle image velocimetry,” *Physics of Fluids* **35** (2023).
- ³⁰C. Lagemann, K. Lagemann, S. Mukherjee, and W. Schröder, “Generalization of deep recurrent optical flow estimation for particle-image velocimetry data,” *Measurement Science and Technology* **33**, 094003 (2022).
- ³¹C. J. Kähler, T. Astarita, P. P. Vlachos, J. Sakakibara, R. Hain, S. Discetti, R. La Foy, and C. Cierpka, “Main results of the 4th international piv challenge,” *Experiments in Fluids* **57**, 97 (2016).
- ³²A. Liberzon, D. Lasagna, M. Aubert, P. Bachant, J. Borg, *et al.*, “Openpiv/openpiv-python: Updated pyprocess with extended area search method,” (2016).
- ³³Z. Xie, H. Wang, and D. Xu, “Spatiotemporal optimization on cross correlation for particle image velocimetry,” *Physics of Fluids* **34** (2022).
- ³⁴P. A. Dellenback, J. Macharivilakathu, and S. R. Pierce, “Contrast-enhancement techniques for particle-image velocimetry,” *Applied optics* **39**, 5978–5990 (2000).
- ³⁵U. Shavit, R. J. Lowe, and J. V. Steinbuck, “Intensity capping: a simple method to improve cross-correlation piv results,” *Experiments in Fluids* **42**, 225–240 (2007).
- ³⁶Y. Lee, S. Zhang, M. Li, and X. He, “Blind inverse gamma correction with maximized differential entropy,” *Signal Processing* **193**, 108427 (2022).
- ³⁷Y. Fan, C. Guo, Y. Han, W. Qiao, P. Xu, and Y. Kuai, “Deep-learning-based image preprocessing for particle image velocimetry,” *Applied Ocean Research* **130**, 103406 (2023).
- ³⁸F. Zhao, Z. Zhou, D. Hung, X. Li, and M. Xu, “Flow field reconstruction from spray imaging: A hybrid physics-based and machine learning approach based on two-phase fluorescence particle image velocimetry measurements,” *Physics of Fluids* **36** (2024).
- ³⁹R. Mejia-Alvarez and K. Christensen, “Robust suppression of background reflections in piv images,” *Measurement Science and Technology* **24**, 027003 (2013).
- ⁴⁰M. A. Mendez, M. Raiola, A. Masullo, S. Discetti, A. Ianiro, R. Theunissen, and J.-M. Buchlin, “Pod-based background removal for particle image velocimetry,” *Experimental Thermal and Fluid Science* **80**, 181–192 (2017).
- ⁴¹L. Wang, C. Pan, J. Liu, and C. Cai, “Ratio-cut background removal method and its application in near-wall piv measurement of a turbulent boundary layer,” *Measurement Science and Technology* **32**, 025302 (2020).
- ⁴²R. J. Adrian and J. Westerweel, *Particle image velocimetry*, 30 (Cambridge university press, 2011).
- ⁴³S. Adatrao and A. Sciacchitano, “Elimination of unsteady background reflections in piv images by anisotropic diffusion,” *Measurement Science and Technology* **30**, 035204 (2019).
- ⁴⁴D. S. Bolme, J. R. Beveridge, B. A. Draper, and Y. M. Lui, “Visual object tracking using adaptive correlation filters,” in *2010 IEEE computer society conference on computer vision and pattern recognition* (IEEE, 2010) pp. 2544–2550.
- ⁴⁵J. F. Henriques, R. Caseiro, P. Martins, and J. Batista, “Exploiting the circulant structure of tracking-by-detection with kernels,” in *European conference on computer vision* (Springer, 2012) pp. 702–715.
- ⁴⁶J. F. Henriques, R. Caseiro, P. Martins, and J. Batista, “High-speed tracking with kernelized correlation filters,” *IEEE Transactions on Pattern Analysis and Machine Intelligence* **37**, 583–596 (2015).
- ⁴⁷S. T. Wereley and C. D. Meinhart, “Second-order accurate particle image velocimetry,” *Experiments in fluids* **31**, 258–268 (2001).
- ⁴⁸A. C. Eckstein, J. Charonko, and P. Vlachos, “Phase correlation processing for dpiv measurements,” *Experiments in Fluids* **45**, 485–500 (2008).

- ⁴⁹M. Shen and H. Liu, "A modified cross power-spectrum phase method based on microphone array for acoustic source localization," in *2009 IEEE International Conference on Systems, Man and Cybernetics* (IEEE, 2009) pp. 1286–1291.
- ⁵⁰K. Chen, Y. Lee, and H. Soh, "Multi-modal mutual information (mummi) training for robust self-supervised deep reinforcement learning," in *IEEE International Conference on Robotics and Automation (ICRA)* (2021).
- ⁵¹E. Delnoij, J. Westerweel, N. G. Deen, J. Kuipers, and W. P. M. van Swaaij, "Ensemble correlation piv applied to bubble plumes rising in a bubble column," *Chemical Engineering Science* **54**, 5159–5171 (1999).
- ⁵²S. Cai, J. Liang, Q. Gao, C. Xu, and R. Wei, "Particle image velocimetry based on a deep learning motion estimator," *IEEE Transactions on Instrumentation and Measurement* **69**, 3538–3554 (2019).
- ⁵³C. Bai, H. Park, C. Y. Ng, and L. Wang, "Classification of gas dispersion states via deep learning based on images obtained from a bubble sampler," *Chemical Engineering Journal Advances* **5**, 100064 (2021).
- ⁵⁴H. Park, C. Bai, C. Y. Ng, and L. Wang, "Bubble image database," (2021).
- ⁵⁵J. Lu, *Research on Variational Optical Flow Particle Image Velocimetry in Hypersonic Flows*, Ph.D. thesis, Huazhong University of Science and Technology (2023).